Supplementary Discussion

Role of I94V in conditional lethality and suppression

The relatively conservative mutation I94V was intentionally introduced into the S1-S2 linker to create a SalI cut site for inserting the S2-S4 mutant library into KAT1. We tested various combinations of single, double, and triple mutants to assess the involvement of I94V in our screens. As expected, the I94V mutation alone did not affect the channel's ability to rescue yeast (data not shown). Without the I94V mutation, W75D but not W75E compromised the ability of KAT1 channels to rescue yeast (Supplementary Table S2). A feature of the model presented in the main text is that I94V is involved in S1-S2 packing, which supports its role in creating synthetic lethality with W75E.

Subunit interactions

We wanted to determine whether the two pairs identified between S4 and S5 correspond to S4 contacting a single S5 segment or the bottom of one S5 and the top of another. The distance between S4 suppressors M169L and S179N is about 17 Å (Cα-Cα), while the distance between the corresponding conditional lethal mutations on S5, H210E and V204E, is about 9 Å within the same subunit and 29 Å between subunits. Due to the length of the side chains involved, either of these scenarios is possible, so we carried out directed screening to determine which is most likely (Supplementary Table S1D). Notably, we tested positions about one helical turn below (L172) the upper S4 suppressor, M169L, and one turn above it (R165) for their ability to suppress the conditional lethality of H210E. Screening with a randomized codon at the R165 position in S4 revealed that R165K suppressed H210E (Fig. 1b), but no such suppressor at L172 was found. The distance between S4 suppressors R165K and S179N is 24 Å supporting the configuration in which S4 makes contact with two different S5 segments in the down state.

As discussed above, we believe that S4 contacts two S5 segments from adjacent subunits. We critically probed this assumption by carrying out two sets of simulations: first, we assumed that all interactions are between the same pair of S4 and S5 segments, and second, we assumed a single S4 contacts two adjacent S5 segments (the result of these simulations is presented in the main text). Representative structures showing the S4 segment in relationship to the central pore from each set of simulations are depicted in Supplementary Fig. 1. The total Cα-Cα distance between the six restraints used in each set of simulations is similar in these models (48 Å versus 45 Å for the best two models in each set). Whereas the S4 helix remains straight when making contacts with two S5 segments (Supplementary Fig. 1a), a large helical bend (> 90°) at position L175 is necessary for spatially matching the pairs of interactions between S4 and the same S5 segment (Supplementary Fig. 1b). This bend is between charged residues R3 and R4 in Shaker-like channels according to alignment A and between R2 and R3 according to alignment B (see Supplementary Fig. 1b) —an unlikely scenario given that the leucine located at the bend in either of the alignments has the second highest helical propensity[1], and S4 is predicted to be highly helical in this region based upon several structure

prediction algorithms[2-4]. Moreover, data presented in the companion paper by Tombola and colleagues are in agreement with the configuration in panel a. Taken together, these considerations suggest that the S4 helix is largely straight in both the up and the down states.

Alignments

The alignment between S4 and S5 segments of KAT1 and Shaker/Kv1.2 is important for our analysis, and the low level of amino acid identity in this region makes aligning difficult. We present two possible alignments of S4 (Supplementary Fig. 1c): the first (A) is deduced from a massive multiple-alignment using clustal-W along with manual adjustments, and the second (B) is based on cysteine accessibility studies. Latorre and colleagues showed that R177C of KAT1 is the deepest arginine site that could be chemically modified from the external solution in the up state[5]. Similar experiments in Shaker revealed that the deepest arginine site is R368[6]. This gives strong experimental evidence for the reliability of alignment B, which we use throughout the main text. However, the conclusions of our manuscript do not depend critically on this choice.

The second question concerns the alignment of S5 segments. In our previous manuscript, we adopted an alignment of KAT1 to Shaker from Shealy *et al.*[7] that is shifted by six residues compared to the one used here (see Supplementary Fig. 1c). The Kv1.2 crystal structure revealed that this alignment provided an exceedingly short S4-S5 linker. Thus, we searched for additional evidence for an alignment. The present alignment is taken from Latorre *et al.*[8], and it has several positive features. First, the S4-S5 linker is comparable in size to the Kv1.2 linker for both S4 alignments above. Second, the extracellular end of the S5 helix of Kv1.2 terminates in a series of charged residues. The present alignment places two proline residues in KAT1 where the termination of Kv1.2 occurs, and given the role of proline residues in terminating helices this supports the present alignment. Finally, sequence analysis of 15 channels closely related to KAT1 shows that there is a sudden increase in sequence variability immediately following the second proline, P226 (data not shown). Highly variable positions often indicate water-accessibility, which would be the case if this proline marks the extracellular end of the S5 helix.

Gating charge calculations

A final test of the model is to compare the predicted voltage sensitivity with the experimentally measured values. To do this, we used Kv1.2 to model the up state of the voltage sensor and the structure suggested by our results to model the down state. While KAT1 is a hyperpolarization-activated channel and Kv1.2 is a depolarization-activated channel, gating charge movement, cysteine accessibility studies, and functional chimeric channels combining KAT1 and *Xenopus* Kv1 sequences suggest that the voltage-sensing mechanism is similar[5,6,9,10]. Homology models in both states were embedded in a low-dielectric, solute-impermeable slab mimicking the lipid environment (Supplementary Fig. 2b), and a membrane potential was imposed on the system through the far-field boundary conditions. We calculated the interaction energy of the S4 positive charges with the membrane potential, and the difference in these energies between the down and up states

to determine the gating charge transfer[11]. Carrying this out using a model of Shaker produced gating charge values of 11.0 (alignment A) or 11.6 (alignment B) using one of two very similar S4 alignments, both very close to the experimental range[12]. The robustness of this result was tested by repeating the process using another KAT1 structure randomly selected from the top 10% of the models to make homology models of Shaker in the down state. The values were 11.1 and 11.4, respectively, with the small variation due to the similarity in S4 orientation among our best models. For models based on structures in Supplementary Fig. 1b in which S4 contacts only a single S5 segment, the gating charge transfer values are 10.1 (alignment A) and 12.1 (alignment B). Both types of models in Supplementary Fig. 1 produce large gating charge values due to the large outward movement of the S4 segment. In these calculations, only the contribution due to a 17-residue span centred on the S4 helix are considered (L358-K374 for Shaker, I166-F182 for KAT1).

Repeating the process with models of KAT1 produced significantly smaller gating charge values of 5.0 (alignment A) or 7.3 (alignment B), compared to gating charge measurements of 5.2 in one study[13] and 3.0 in another[5].

The sensitivity of the Shaker channel to voltage is remarkable[14], and it is of primary interest that our model exhibits this sensitivity by producing large gating charge transfers. However, it has been shown that, of the key acidic residues in S2 (E283 and E293) and S3 (D316), neutralization of E293 but not E283 or D316 influences the gating charge[15]. To determine the contribution of these negative residues, we assessed the effect of the S2 charges, E283 and E293, on our calculations. For our Shaker models, E283 and E293 together contribute only ~0.5 charges to the total gating charge. While this is consistent with the result that E283Q has little effect on the magnitude of the gating charge, ostensibly it is at odds with the result that E293Q, 2 helical turns down from E283, reduces the gating charge by 6.3 charges per channel[15], or 1.6 charges per subunit. Clearly this latter result cannot solely be interpreted in terms of the motion of E293 through the membrane electric field, since this value cannot physically exceed unity. One possible explanation is that the lack of a charge at E293 energetically biases the conformation of the voltage sensor so that it does not undergo its full range of motion under the applied membrane potential and hence, the gating charge is greatly reduced. While this is speculative, a detailed energetic analysis of how each residue contributes to the total gating charge is needed to determine if this can explain the discrepancy between the current theoretical analysis and experiment.

Coupling voltage sensor movements to channel gating

Whereas the hydrophobic interactions between the S4-S5 linker and S6 in Kv1.2 suggest that the cytoplasmic extension of the voltage sensor segment S4 and the pore-lining helix S6 remain associated in both open and closed Kv1.2 channels, a model of the KAT1 S4-S5 linker and the S6 cytoplasmic extension based on the Kv1.2 structure places arginines from both segments in close apposition (Supplementary Fig. 3). Such a configuration is unlikely to be realized. Rather, when the S4-S5 linker is in the up state, electrostatic repulsion between S6 and the linker may induce dissociation of these regions leading to channel closure.

To assess the possible interactions between S6 and the S4-S5 linker when the VSD is in the down state, we used Modeller[16] to introduce the S4-S5 linker to the down state KAT1 transmembrane structure that we constructed from our experimental constraints. We imposed alpha-helical restraints on the linker from L185 to C198. The model presented in Supplementary Fig. 3 shows that two arginines (R190 and R197) on the S4-S5 linker, which point toward S6 in the up state according to the Kv1.2 structure, are pointing away in the down state. Meanwhile, this rotation of the linker places an aspartate (D188) close to R310 on S6. While this model lacks experimental restraints and is therefore tentative, such favourable electrostatic interactions may cause an outward motion of the C-terminus of S6 toward the S4-S5 linker and open the channel.

Our model for the gating of hyperpolarization-activated KAT1 channels based on electrostatic interactions between the S4-S5 linker and S6 is in agreement with recent experiments on spHCN channels that also activate upon hyperpolarization[17]. Prole and Yellen reported that crosslinking the S4-S5 linker to S6 of the spHCN channel, thereby forcing the cytoplasmic end of S6 to track the S4-S5 linker during VSD movements, converts the channel into a depolarization-activated channel[17]. It will be interesting in future studies to examine the possibility of two evolutionarily conserved mechanisms for voltage-gating: one where persistent association of S6 with the S4-S5 linker leads to channel opening as the VSD moves upward upon depolarization for depolarization-activated channels, and another where state-dependent interactions allow S6 to approach the S4-S5 linker only when VSD is in the down state thereby opening the channel upon hyperpolarization for hyperpolarization-activated channels.

Supplementary Methods

Molecular Biology and Library Construction. Yeast screens and selection were carried out as previously described, as were the construction of the S1-S3 and S4 libraries[18]. For the S2-S4 library, a SalI cut site was made at residue I94 thereby mutating this residue to valine, and a silent BamHI cut site was engineered in at residue W195. This construct gave the same phenotype as wild-type in the yeast assay (data not shown). The stuffer sequence containing the N- and C-terminus (residues 1-96 and 192-414 linked with a GGSGG sequence in between) of Kir 3.2 was inserted between the SalI-BamHI cut sites, providing a non-functional background and negative control cloning vector for library construction (KAT1-S2-S4-stuffer) in the same way the KAT1-S1-S3-stuffer and KAT1-S4-stuffer constructs were for the S1-S3 and S4 libraries as previously described[18]. The stuffer negative control shown in the figures is the KAT1-S4-stuffer. All constructs were verified by fluorescence sequencing. The error-prone PCR and library construction for the S2-S4 library were performed as previously described[18], with flanking primers containing the SalI and BamHI cut sites for proper ligation into the parent vector.
All targeted mutations were made using the QuikChange site-directed mutagenesis kit (Stratagene, LaJolla, CA). Randomized codons were created using the QuikChange kit with primers containing NNN (25% A,C,G,T at each site) yielding 64 possible codons or NN(G/C) yielding 32 possible codons and all amino acids.

Constructing the models. Modeller[16] was used to construct an open state model of the KAT1 pore region based on the Kv1.2 crystal structure[19] using the alignment in Supplementary Fig. 1c. Alignment of the S5 segment follows from the work of Latorre *et al.*[8], while the inner helix alignment was adapted from Shealy *et al.*[7]. We repeated this process for the four transmembrane segments S1-S4 ignoring the soluble loop regions. Both S1 and S3 are represented as polyalanine helices in the Kv1.2 structure, so an alignment is not possible, and the structure is used simply as a template for the secondary structure. S4 was constructed using either the A or B alignment in Supplementary Fig. 1c. These four helices were initially aligned with, and centred on, the pore axis in a manner consistent with known membrane topology. The S4 helix was then translated away from the pore domain, randomly rotated about its axis, tilted off-axis up to ±45°, and then rotated in the x-y plane about its centre. This was repeated for segments S1-S3, which were disposed around S4 in an order consistent with the helix order seen in the Kv1.2 structure.

Several sets of force restraints were then placed upon the initial, randomized structure:

1) Harmonic restraints were placed between six of the eight pairs identified in the screen and marked in Table 1, using a force constant of 4 kcal/mol/Å^2.

2) Our screen revealed no structural constraints for the S3 segment. To model this helix, an alignment of 30 homologous KAT1 channels was carried out from which we determined that several residues are strictly conserved yet others are highly variable. Forces were placed upon these residues either attracting them to the other VSD transmembrane elements or repelling them, with the notion that

high conservation designates protein-packing faces of the S3 helix[20]. Residues were designated as strictly conserved, highly conserved, or variable and force constants –0.008, -0.001, and 0.008 kcal/mol/Å^2 were placed on each, respectively. Harmonic restraints were also placed between the N-terminal end of S3 and the C-terminal end of S2 as well as the C-terminal end of S3 and the N-terminal end of S4.

3) Dihedral restraints were placed along the backbone of segments S1-S4 to maintain secondary structure during the simulations.

4) All backbone atoms of the central pore were fixed. S1-S4 side chains not involved in pair interactions were modelled as glycine.

Molecular dynamics simulations using NAMD 2.5 were performed at high temperature, 600K, for a total of 80 ps with a reduced 1.5 fs time step allowing the protein complex to pack together[21]. This was followed by minimization of the entire system. 200 simulations were carried out with different initial configurations of the helices S1-S4, and each final structure model was scored based on the Cα-Cα distance between lethal and suppressor residues. Our methodology closely follows that used by Roux[22].

Electrostatic calculations. All electrostatic calculations were carried out with the program APBS[23] using the PARSE parameter set for the protein partial charges[24]. The effect of the membrane potential and membrane was accounted for as described by Grabe and colleagues[11]. The dielectric value of the water, protein, and membrane were assigned values of 80, 10, and 2, respectively. The aqueous environment was modelled with a symmetric ionic solution of 100 mM. Numerically, the linearized Poisson-Boltzmann equation was solved with two levels of focusing with a spatial discretization of 0.6 Å per grid point at the finest level.

Supplementary Figures

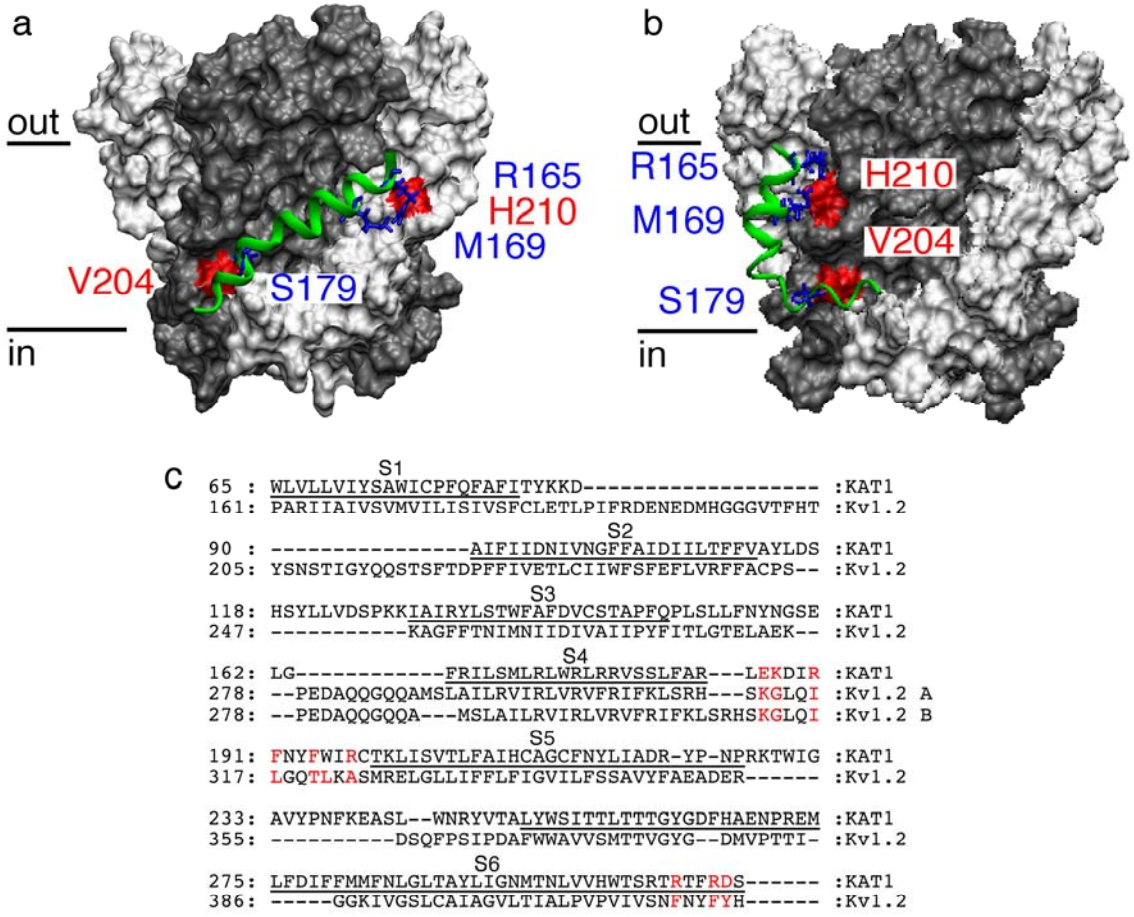

Supplementary Figure 1 | Two down state models of KAT1. Two sets of models were generated from the results of the yeast screen assuming S4 contacts a single S5 segment or two S5 segments. The central pore is shown as a surface, with alternating subunits coloured grey and white. A single, S4 segment (green) is shown in each panel. **a,** We assumed that the N-terminus of S4 contacts H210 in the white subunit and the C-terminal end contacts V204 of the neighbouring grey subunit. **b,** All interactions are between the same S4 and S5 segments. This produces a large kink in the centre of the S4 helix, but otherwise satisfies the experimental constraints quite well. **c,** The alignment of KAT1 to Kv1.2. Two possible alignments of the S4 segment are provided. Transmembrane domains are indicated above the sequence, and only underlined residues were used in constructing models. Positions coloured red indicate interacting residues between the S4-S5 linker and S6 in the Kv1.2 crystal structure[25]. Note that while many of these residues are hydrophobic in Kv1.2, they are highly charged in KAT1 suggesting that the mechanical coupling between the S4-S5 linker and the central pore may be electrostatic in KAT1 rather than hydrophobic (see Supplementary Fig. 3). Note that R294, R297, R300, and R303 in Kv1.2 are commonly referred to as R1, R2, R3, and R4, respectively.

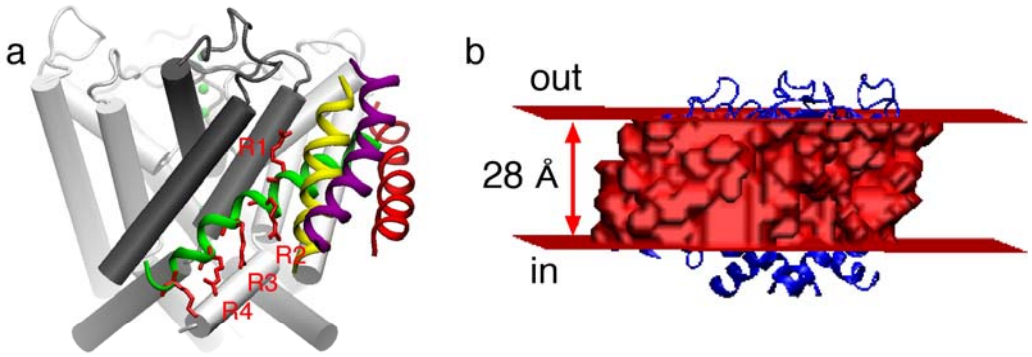

Supplementary Figure 2 | Gating charge calculations using the Shaker channel. a, Homology model of Shaker constructed on the down state model of KAT1 from Fig. 2 using alignment B from the Supplementary Discussion. The first five charged groups are represented explicitly (red sticks), and the first four are labeled R1-R4. R1 and R2 have intimate contact with S1, but the last residues point down into the cytoplasmic space. Directly behind the VSD is the neighbouring central pore subunit (grey) while its own subunit is to the right (white). **b,** The channel (blue) was embedded in a low dielectric slab (red) corresponding to the lipid bilayer, and a membrane potential was applied across the system. The slab is 28 Å thick and bounded above and below by water. Gating charge transfers were determined for the transition from the down state to the up state based on such calculations.

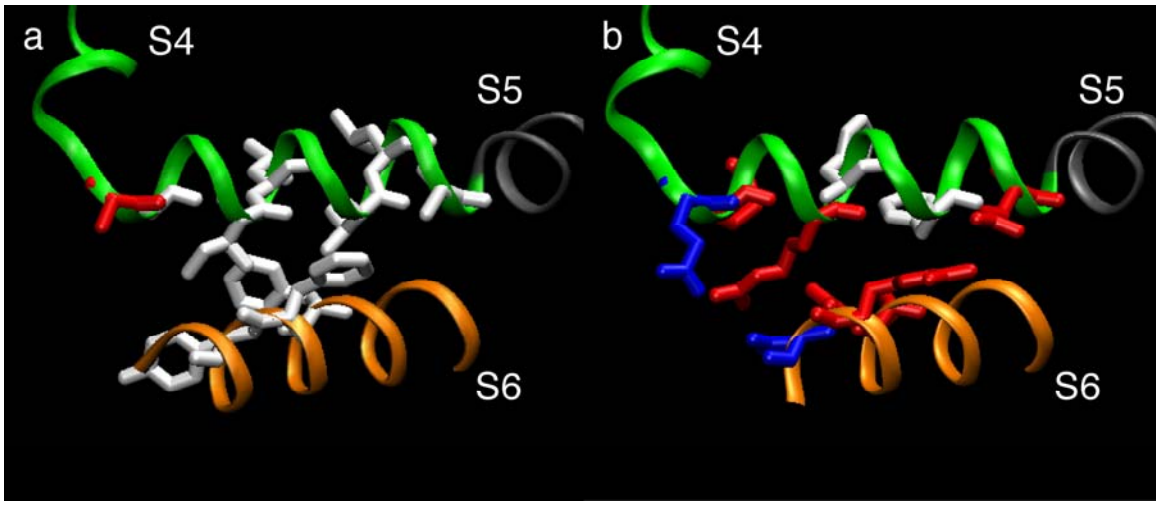

Supplementary Figure 3 | Connection between S4-S5 linker and S6. The S4-S5 linker (top, green) of Kv1.2 **(a)** and KAT1 **(b)** together with the C-terminal end of S6 (bottom, gold) are pictured looking from the cytoplasm. Kv1.2 is the crystal structure solved by Long *et al*.[19], while KAT1 is an up state model based on the Kv1.2 structure using alignment B in Supplementary Fig. 1c and constructed using Modeller[16]. Residues at the interface of S6 and the S4-S5 linker are represented explicitly. These residues are coloured red in Supplementary Fig. 1c. Acidic residues are blue, basic residues red, and neutral residues white. All white residues are hydrophobic except for the S6 residue Y417 in Kv1.2, which is polar but aromatic. Clearly, the chemistry of the Kv1.2 interface is much more hydrophobic than the KAT1 interface, which has many arginines in close proximity. When the S4-S5 linker is in the up state, the central pore of KAT1 is closed. The energetic considerations suggest that the proximity of arginines on adjacent segments of KAT1 in panel b based on the Kv1.2 structure is in fact a high energy state, implying that the open channel conformation in this KAT1 model is unrealistic, and repulsive electrostatic forces between S6 and S4-S5 linker residues will induce a closing of the central pore when the VSD is in the up state.

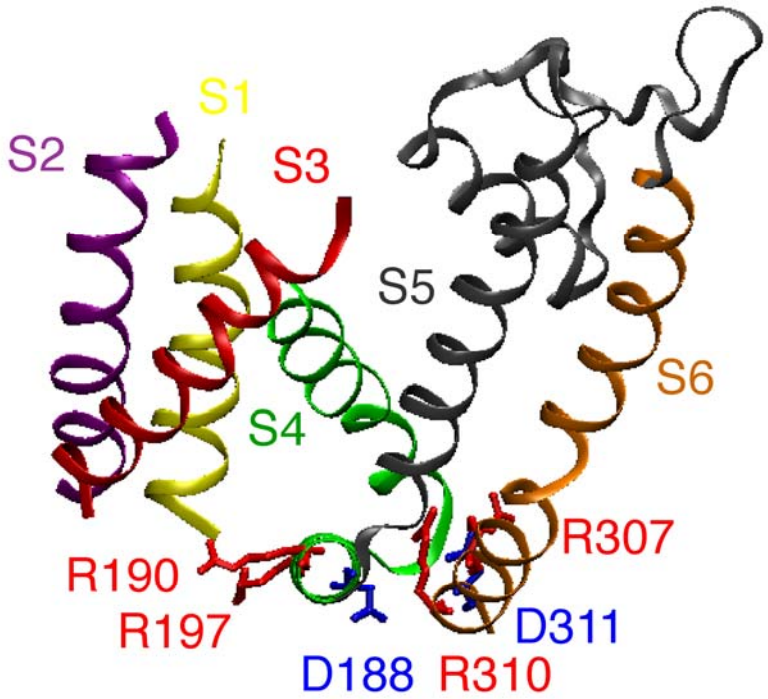

Supplementary Figure 4 | A down state model of the S4-S5 linker. The S4-S5 linker region was modelled onto the KAT1 structure in Fig. 2 using Modeller[16] with the restraint that the linker be helical. The figure is positioned as in Fig. 2a and coloured as in Supplementary Fig. 3. This view is looking down the S4-S5 linker from the membrane. Compared to Supplementary Fig. 3b, this structure represents a rotation of the arginines on the S4-S5 linker, R190 and R197, away from the interface, which may allow for favourable interactions between the C-terminus of S6, R310 and R307, with D188 on the linker. This may result in an outward radial motion of S6 leading to channel opening. This model of the linker placement lacks experimental verification, and should therefore be regarded as tentative.

Supplementary Tables

Supplementary Table 1 | Summary of screens performed to identify interactions between transmem

a, S1-S3 screen

Putative TM region of Conditional Lethal	*Conditional Lethal*	*Library Complexity*	*# Screened*	*Estimated % Rescue*	*% Unselected AA changes*	*% Unselecte b.p. change*
S4	**R171E**	1.5×10^5	9279	1.70	4.3-6	2.2-3
S4	**R174E**	1.2×10^4	10206	0.27	6-6.3	3.0
S4	**L175N**	9.4×10^3	2067	0.01	6.0	3.0
S4	**L175H**	1.6×10^4	1474	0.00	6.0	3.0
S4	**L175P**	1.1×10^4	1714	0.00	6.0	3.0
S4	**V178N**	1.7×10^4	1948	0.20	6.0	3.0
S5	**F207D**	1.8×10^4	2724	0.00	6.0	3.0
S5	**F207K**	1.0×10^3	531	0.00	6.0	3.0
S5	**F207R**	1.7×10^4	2508	0.00	6.0	3.0
S5	**F215R**	5.2×10^3	1991	0.00	6.0	3.0
S6	**N284K**	3.1×10^3	1720	0.00	6.0	3.0
S6	**N284R**	4.2×10^3	1578	0.00	6.0	3.0

b, S4 screen

Putative TM region of Conditional Lethal	*Conditional Lethal*	*Library Complexity*	*# Screened*	*Estimated % Rescue*	*% Unselected AA changes*	*% Unselecte b.p. change*
S5	**F207D**	1.2×10^3	1007	0.00	5.8	3.1
S5	**F207K**	1.4×10^3	873	0.00	5.8	3.1
S5	**F207R**	8.0×10^2	876	0.00	5.8	3.1
S5	**F215R**	5.2×10^3	4536	0.00	5.8-7.7	3.1-3.5
S6	**N284K**	1.0×10^4	2715	0.00	5.8	3.1
S6	**N284R**	1.5×10^4	2231	0.00	5.8-7.7	3.1-3.5
S6	**N284P**	1.0×10^2	548	0.00	7.7	3.5

c, S2-S4 screen

Putative TM region of Conditional Lethal	*Conditional Lethal*	*Library Complexity*	*# Screened*	*Estimated % Rescue*	*% Unselected AA changes*	*% Unselecte b.p. change*
S1	**W75E** + **I94V**	8.4×10^2	2620	0.30	5.2	2.6
S1	**W75D** + I94V	4.2×10^3	3646	0.10	5.2	2.6
S1	**W75K** + I94V	1.7×10^3	1777	0.00	5.2	2.6
S1	**W75R** + I94V	3.6×10^3	2697	0.00	5.2	2.6

d, Screens against a specific amino acid

Putative TM region of Conditional Lethal	*Conditional Lethal*	*Library Complexity*	*# Screened*	*Estimated % Rescue*	*Site of Random Mutation*	*Putative TM region of Site Random Mutation*
S4	**L175N**	960	353	0.00	V204X	S5
S4	**L175N**	1287	133	0.00	F207X	S5
S4	**L175N**	1008	176	0.00	H210X	S5
S5	**V204E**	1035	2481	0.00	R165X	S4
S5	**V204E**	1364	5223	0.00	L172X	S4
S5	**H210E**	128	2405	0.25	R165X	S4
S5	**H210E**	59	658	0.00	L172X	S4
S6	**F283P**	638	532	0.00	R165X	S4
S6	**N284K**	842	1114	0.00	M169X	S4
S6	**N284K**	1300	557	0.00	L172X	S4
S6	**N284P**	200	91	0.00	M169X	S4
S6	**N284P**	768	458	0.00	L172X	S4
S6	**N284R**	133	13*	0.00	M169X	S4

The putative transmembrane region, the conditional lethal, library complexity, number of yeast colonies screened, the estimated percent rescue, the percent amino acid (AA) changes in the unselected library, the percent base pair (b.p.) changes in the unselected library, and the suppressor mutation(s) are given. Conditional lethal mutations are in red and specific second-site suppressor mutations in blue. Screens of conditional lethal mutations against randomized regions of S1-S3 (**a**), S4 (**b**), and S2-S4 (**c**) are shown. **d,** A summary of the screens performed looking for a second-site suppressor of a particular conditional lethal at a specific site. The site of the randomized codon and its putative transmembrane segment location are given.

Supplementary Table 2 | Analysis for the requirement of the I94V mutation.

Putative TM Region	*Mutations*	*0.4 mM K+*
S1	**W75E**	+
S1 + S2	**W75E** + **I94V**	-
S1 + S2	**W75E** + **I94V** + **N99D**	+
S1	**W75D**	-
S1 + S2	**W75D** + **I94V**	-
S1 + S4	**W75D** + **M169L**	+
S1 + S2 + S4	**W75D** + **I94V** + **M169L**	+

A detailed examination of the role of the I94V mutation created by the SalI cut site for the S2-S4 mutant libraries. The phenotype in the K^+ transporter deficient yeast strain on 0.4 mM K^+ plates is represented by + for yeast growth and – for no yeast growth. W75E alone rescues yeast growth on 0.4 mM K^+ selective plates, but W75E+I94V is conditionally lethal. W75D is conditionally lethal with or without I94V. The suppressor, M169L, was discovered in conjunction with W75D+I94V; however, I94V is not required for suppression.

Supplementary Movie

A movie of the down and up gating states has been provided. The channel is viewed from the extracellular space, and subunits are coloured silver and blue, alternatively. A potassium ion (purple) can be viewed in the centre of the channel, and the central pore remains unchanged in both states since the up state is based on the open Kv1.2 channel and the down state is based on the open KAT1 channel. The VSDs undergo large rearrangements at the edge of the channel, and they are next to the pore domain of the neighbouring subunit in the up state and their own subunit in the down state.

References

1 Pace, C.N. & Scholtz, J.M. *Biophys. J.* **75,** 422-427 (1998).
2 Adamczak, R., Porollo, A., & Meller, J. *Proteins* **59,** 467-475 (2005).
3 Jones, D.T. *J. Mol. Biol.* **292,** 195-202 (1999).
4 Ouali, M. & King, R.D. *Protein Sci.* **9,** 1162-1176 (2000).
5 Latorre, R. *et al. J. Gen. Physiol.* **122,** 459-469 (2003).
6 Baker, O.S., Larsson, H.P., Mannuzzu, L.M., & Isacoff, E.Y. *Neuron* **20,** 1283-1294 (1998).
7 Shealy, R.T., Murphy, A.D., Ramarathnam, R., Jakobsson, E., & Subramaniam, S. *Biophys. J.* **84,** 2929-2942 (2003).
8 Latorre, R., Munoz, F., Gonzalez, C., & Cosmelli, D. *Mol. Membr. Biol.* **20,** 19-25 (2003).
9 Mannikko, R., Elinder, F., & Larsson, H.P. *Nature* **419,** 837-841 (2002).
10 Cao, Y., Crawford, N.M., & Schroeder, J.I. *J. Biol. Chem.* **270,** 17697-17701 (1995).

11 Grabe, M., Lecar, H., Jan, Y.N., & Jan, L.Y. *Proc. Natl. Acad. Sci. USA* **101,** 17640-17645 (2004).

12 Schoppa, N.E., McCormack, K., Tanouye, M.A., & Sigworth, F.J. *Science* **255,** 1712-1715 (1992).

13 Hoshi, T. *The Journal of general physiology* **105,** 309-328 (1995).

14 Sigworth, F.J. *Nature* **423,** 21-22 (2003).

15 Seoh, S.A., Sigg, D., Papazian, D.M., & Bezanilla, F. *Neuron* **16,** 1159-1167 (1996).

16 Sali, A. & Blundell, T.L. *J. Mol. Biol.* **234,** 779-815 (1993).

17 Prole, D.L. & Yellen, G. *J. Gen. Physiol.* **128,** 273-282 (2006).

18 Lai, H.C., Grabe, M., Jan, Y.N., & Jan, L.Y. *Neuron* **47,** 395-406 (2005).

19 Long, S.B., Campbell, E.B., & Mackinnon, R. *Science* **309,** 897-903 (2005).

20 Minor, D.L., Jr., Masseling, S.J., Jan, Y.N., & Jan, L.Y. *Cell* **96,** 879-891 (1999).

21 Kale, L. *et al. J. Comp. Phys.* **151,** 283-312 (1999).

22 Roux, B. *Novartis Found. Symp.* **245,** 84-101; discussion 101-108, 165-108 (2002).

23 Baker, N.A., Sept, D., Joseph, S., Holst, M.J., & McCammon, J.A. *Proc. Natl. Acad. Sci. USA* **98,** 10037-10041 (2001).

24 Sitkoff, D., Sharp, K.A., & Honig, B. *J. Phys. Chem.* **98,** 1978-1988 (1994).

25 Long, S.B., Campbell, E.B., & Mackinnon, R. *Science* **309,** 903-908 (2005).